NGGAN: Noise Generation GAN Based on the Practical Measurement Dataset for Narrowband Powerline Communications

Ying-Ren Chien, *Senior Member, IEEE*, Po-Heng Chou, *Member, IEEE*, You-Jie Peng, Chun-Yuan Huang, Hen-Wai Tsao, *Life Member, IEEE*, and Yu Tsao *Senior Member, IEEE*

***Abstract*—To enhance impulse noise processing for narrowband power line communications (NB-PLC) transceivers, capturing comprehensive statistics of non-periodic asynchronous impulsive noise is a critical issue. However, the existing mathematical noise generative models only capture part of the characteristics of the additive noise. Therefore, we propose a generative adversarial network (GAN) called noise generation GAN (NGGAN) that learns the complicated characteristics in the practically measured noise samples for data augmentation. To closely match the statistics of complicated noise over the NB-PLC systems, we measured the NB-PLC noise via the analog coupling and bandpass filtering circuits of a commercial NB-PLC modem to build a realistic dataset. Specifically, the approaches of NGGAN design based on the practically measured dataset are as follows: (i) we design the length of input signals that the NGGAN model can fit to facilitate cyclo-stationary noise generation, (ii) Wasserstein distance is used as a loss function to enhance the similarity between the generated noise and training dataset, and it ensures that the sample diversity is sufficient for various applications. (iii) To measure the similarity performances of GAN-based models based on the mathematical and practically measured datasets, we perform quantitative and qualitative analyses. The training datasets include (1) a piecewise spectral cyclo-stationary Gaussian model (PSCGM), (2) a frequency-shift filter (FRESH), and (3) practical measurements from NB-PLC systems. Simulation results demonstrate that the proposed NGGAN trained by waveform characteristics is closer to the practically measured dataset in terms of the quality of the generated noise. The principal component analysis (PCA) scatter and Fréchet inception distance (FID) analysis have shown that the NGGAN is able to generate the best fidelity and the highest diversity noise samples compared to other comparative GAN-based models.**

***Index Terms*—Cyclo-stationary noise, generative adversarial network (GAN), measurement dataset, noise model, narrowband powerline communications (NB-PLC), process innovation.**

Manuscript received April 9, 2024; revised August 18, 2024; accepted September 6, 2024. This work was supported in part by the National Science and Technology Council (NSTC) of Taiwan under Grant 109-2221-E-197-026, 112-2221-E-197-022, and 113-2926-I-001-502-G, and Academia Sinica, under Grant 235g Postdoctoral Scholar Program *(Corresponding author: Po-Heng Chou)*.

Ying-Ren Chien is with the Adaptive & Autonomous Communication Lab., Department of Electrical Engineering, National Ilan University, No. 1, Sec. 1, Shen-Lung Rd., I-Lan City, 26041, Taiwan (e-mail: yrchien@niu.edu.tw).

Po-Heng Chou and Yu Tsao are with the Research Center for Information Technology Innovation (CITI), Academia Sinica, Taipei, 11529, Taiwan (e-mail: d00942015@ntu.edu.tw; yu.tsao@citi.sinica.edu.tw).

You-Jie Peng and Hen-Wai Tsao are with the Graduate Institute of Communication Engineering, College of Electrical Engineering and Computer Science (GICE), National Taiwan University (NTU), Taipei, 10617, Taiwan (e-mail: roger851122@gmail.com; tsaohw@ntu.edu.tw).

Chun-Yuan Huang is with the Institute of Communication Engineering (ICE), National Sun Yat-sen University (NSYSU), Kaohsiung, 80424, Taiwan (e-mail: sdff6842@gmail.com).

I. Introduction

NARROWBAND powerline communication (NB-PLC) [1]–[3] is one of the potential physical layer solutions for smart grid, smart home, and indoor positioning applications [4]. However, NB-PLC easily suffers from noise because it is designed for power delivery rather than signal transmission [5]. Measuring the complicated noise in NB-PLC is essential to describe the noise model. A lax and unrealistic noise model may lead to an overly optimistic performance concerning the detection probability [1], data rate [2], and attenuation [2], [3]. Therefore, modeling the noise of NB-PLC to facilitate the physical design of transceivers [6] and network protocols [7] so that the robustness against noise is objectively evaluated [8]. The channel disturbances on NB-PLC systems have been explored in [9], [10]. When employing different additive noise models, the corresponding bit error rate (BER) performance results are observed [5]. Consequently, if the noise generation model fails to accurately represent the majority of the noise, the transceiver design may become excessively optimistic and compromise robustness.

Additive noises in NB-PLC systems (hundreds of Hz to several MHz) are categorized in [11] as follows: (1) colored background noise (CBG), (2) narrowband noise (NBI), (3) periodic impulsive noise asynchronous to the mains frequency (PINS), (4) periodic impulsive noise synchronous to the mains frequency (PINAS), and (5) asynchronous impulsive noise (APIN). The dominant noise in NB-PLC systems is PINS [12]. However, CBG and NBI may not be disregarded [13]. The survey works to model NB-PLC noise had been investigated in [14]. Most previous studies used curve-fitting to establish mathematical models of NB-PLC noise. First, CBG was characterized by one or two dimensions. In the one-dimensional model of CBG, a zero-mean Gaussian distribution with frequency-dependent variance is used to model the probability density function (PDF). In the two-dimension model of CBG, Rayleigh or Nakagami-m distributions were used to model the probability density function (PDF) in the time domain, and a negative exponential decaying form was used to fit the power spectrum density (PSD) in the frequency domain. Next, NBI was characterized by a log-normal distribution in the time domain and the PSD can be modeled by a sum of multiple Gaussian-like functions in the frequency domain. Then, PINS or PINAS can be modeled by a cyclo-stationary Gaussian process generated from a set of frequency-shift (FRESH) filters [15] or a set of parameterized

spectral and temporal shaping filters [16]. Different from PINS and PINAS, the duration and inter-arrival time of APIN are random variables. Thus, APIN has a high degree of random variability.

However, the existing works can only capture part of the characteristics of the additive noise. Because non-periodic asynchronous noise exhibits a high degree of random variability in the duration and inter-arrival time, to the best of our knowledge, there is no single model that can be used to represent all kinds of noise mentioned above. Even if it is possible to combine individual models into a composite model, time synchronization among the sub-models could be a severe problem [17]. Even worse, some noise measurements are costly, such as for multi-phase powerline networks and large-scale distributed powerline networks. Thus, a data-driven modeling approach is suitable for modeling the noise characteristics. Therefore, it is a challenge to accurately capture the trajectories of practical NB-PLC noise by using a mathematical model (e.g., piecewise spectral cyclo-stationary Gaussian model (PSCGM) [18] or FRESH [16]).

Recently, one of the deep learning (DL) models called generative adversarial network (GAN) [19] has proven particularly effective in synthesizing data that is unidentified from measured data. The DL-based approach could reduce the cost of some costly measurements that are needed [20], [21]. For example, electromagnetic interference (EMI) [22], multiple-phase powerline networks [14], [23], long-term noise characterization [24], large-scale distributed powerline networks [25], [26], cyclic frequency offset issues [27], and so on. When the amount of training data is insufficient, the performance of the DL model is poor and overfitting easily [20], [28]. Therefore, increasing the amount of training data is required for generalizability and to avoid overfitting. To address this issue, data augmentation by using GAN is essential. In certain applications, e.g., data processing at end-user devices via mobile edge servers for enhanced quality of service, gathering sufficient training data is challenging due to privacy concerns and cost constraints [29]. In addition, the discrepancy between real and generated data can be considered a valuable source of diversity. To enhance the diversity within the training dataset, data augmentation by employing GAN is also a desirable solution. Consequently, we emphasize comparing the proposed GAN-based model to other GAN-based models.

For modeling complex NB-PLC noise, we propose a GAN-based model named noise generation GAN (NGGAN), which is inspired by the works [30], [31]. The proposed NGGAN, which is a data-driven DL-based approach, aims to generate noise samples that have complicated noise statistics and are not easily captured by some existing noise models. Simulation results have confirmed that the proposed NGGAN can generate noise samples with statistics similar to the original dataset while maintaining a certain level of diversity.

From the measurement perspective, the proposed NGGAN can be used to model complex noise traces for NB-PLC systems and may prove to be a more efficient learnable data augmentation than traditional model-based methods. It could offer significant advantages in training DL-based NB-PLC transceivers [32] that consider the impact of the complicated statistics of the noises for NB-PLC systems [33]. The idea can be extended to the development of consumer electronics devices that suffer from complicated noise [34].

The main contributions of this work are summarized as follows:

- To closely match the statistics of complicated noise over the NB-PLC systems, we measured the NB-PLC noises via the analog coupling and bandpass filtering circuits of a commercial NB-PLC modem to build a realistic dataset [35] from different scenarios involving fans, lamps, and power suppliers [4].
- To precisely extract the features of the NB-PLC noise waveform, the length of the input data is determined based on the cyclo-stationary property.
- To enhance the similarity between the generated noise and training, Wasserstein distance is used to replace Kullback–Leibler (KL) divergence as the loss function of the original GAN to enhance the similarity between the generated noise and three datasets, which is (i) PSCGM, (ii) FRESH, and (iii) practical measurements from an NB-PLC network (The three datasets are available on IEEE DataPort [35]).
- To measure the similarity performances of GAN-based models, several performance metrics are adopted, including (1) maximum value, (2) mean value, (3) energy value, (4) standard deviation, (5) skewness, (6) kurtosis, (7) the number of peaks larger than the certain threshold value, (8) skewness of auto-correlation, (9) kurtosis of auto-correlation, (10) cyclic spectral density (CSD), (11) cyclic spectral coherence (CSC), (12) principal component analysis (PCA), and (13) Fréchet inception distance (FID).
- Simulation results demonstrate the proposed NGGAN is a more efficient data augmentation approach than other GAN-based models to improve its robustness against noise [33] for NB-PLC transceiver design.
- The Python source codes are provided on GitHub[1].

The remainder of this paper is organized as follows: Section II introduces related works on the modeling of NB-PLC noise. Section III describes the proposed NGGAN model. Section IV starts by outlining the performance metrics, followed by a presentation of the datasets and the noise measurements in NB-PLC networks. Section V examines both qualitative and quantitative analysis of noise generated by various GAN models developed for NB-PLC systems. Conclusions are summarized in Section VI.

II. Related Works

In this section, we review the related works about the NB-PLC noise model with the cyclo-stationary properties. First, the PSCGM is introduced, which has been adopted as the standard noise model under IEEE 1901.2 [18, Annex D.3]. Second, the FRESH filter, a parametric approach, is presented [16]. Finally, GAN-based works for generating NB-PLC noise are examined.

[1]https://github.com/yrchien/NGGAN

A. PSCGM Modeling

The IEEE standard 1901.2 [18] proposed the PSCGM model that includes three main components: random background noise, periodic impulsive noise, and random impulse noise, according to the field measurements over low-voltage (LV) sites. The PSCGM divides each period of cyclo-stationary noise into two or three regions to which specific temporal shaping and spectral shaping filters are assigned [36].

However, the PSCGM is measured by using two-dimensional amplitude spectrograms of cyclo-stationary noise to visually distinguish different regions [36], such as the number and size of pulses. Therefore, it does not consider the correlation of Gaussian noise between different regions.

B. FRESH Filter-based Modeling

The noise traces generated by a set of FRESH filters [15] can be categorized into three classes based on the standard deviation in one slot. A set of parameterized spectral and temporal shaping filters [16] is provided for the generated cyclo-stationary noise, using white Gaussian noise as the excitation input. The input is first transformed into the frequency domain using the fast Fourier transform (FFT) to undergo shaping by two asymmetric double-sided exponentially decay functions (i.e., spectral shaping filters). The frequency-shaped signal is subjected to the inverse FFT to obtain a sequence in the time domain, which is subjected to temporal shaping using a symmetric double-sided exponential decay function.

Typically, the assessment of the FRESH filter-based model involves employing the normalized mean-square error (MSE). An effective strategy to reduce normalized MSE is to augment both the quantity and size of FRESH filters. Nonetheless, implementing the FRESH model proves challenging due to the substantial number of parameters associated with each filter. Consequently, the elevated complexity of the FRESH model results in an extended duration for noise generation, as highlighted in [16].

C. GAN-based Modeling

GAN [19] is widely used to extract the features with structural properties within a dataset and to synthesize samples with statistical properties similar to those of training samples [30], [31], [37]–[41]. An effective GAN model for time-series data should maintain temporal dynamics, ensuring that generated sequences uphold the original relationships between variables over time [40]. However, it is difficult to converge for training GAN until the advent of unsupervised learning in the form of deep convolutional GAN (DCGAN) [37], which are characterized by the use of a convolutional layer in the generator and a convolutional-transpose layer in the discriminator. DCGAN converges more easily than the original GAN, while the batch normalization layer enhances stability. In addition, DCGAN uses the short-time Fourier transform (STFT) to transform noise traces into a two-dimensional amplitude spectrogram in the DCGAN [30]. Then, DCGAN uses the Griffin-Lim algorithm [42] to transform the two-dimensional spectrogram into a one-dimensional time-domain sequence. However, the Griffin-Lim algorithm leads to phase deviations in the time-domain sequence, such that the statistical characteristics differ considerably from the practical NB-PLC noise. Thus, it leads to the poor performance of DCGAN in generating cyclo-stationary noise [38]. SpecGAN further improves the performance of DCGAN by using the Wasserstein distance [38], [41] as the loss function.

In our previous work [31], we propose a novel end-to-end GAN model called the phase-learned SpecGAN (PL-SpecGAN) to account for phase spectrum without using phase estimation. PL-SpecGAN further incorporates phase data related to noise signals within a SpecGAN to combine phase and amplitude information simultaneously. It also resolves phase deviation problems by using the Griffin-Lim algorithm for the inverse STFT operation. When dealing with periodic data, the learning performance of the GAN can be improved by increasing the length of the training data. Inspired by the literature [39], we reduced the dimension of the convolutional layer from two dimensions to one and extended the length of the feature filter for the proposed NGGAN. On the other hand, we adopted the frequency-domain version of the SpecGAN (FD-SpecGAN) [37], with modifications to the architecture of the generative and discriminative models to fit our previous framework [31]. We compare the performance of DCGAN, PL-SpecGAN, FD-SpecGAN, and NGGAN by using three kinds of datasets.

III. Proposed NGGAN and Training Processing

In this section, we introduce the proposed NGGAN and its training processing. Fig. 1 depicts the GAN-based model architecture. GAN consists of a generative (G) model, responsible for capturing the data distribution, and a discriminative (D) model, which determines whether the samples are training data or generated data from the G model.

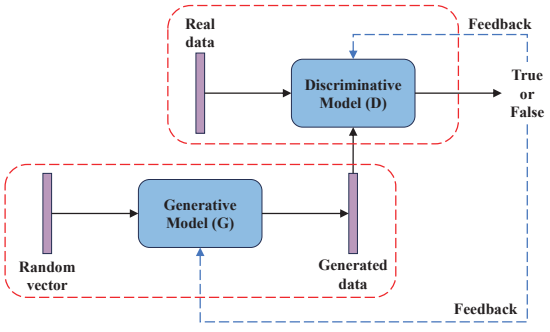

Fig. 1. The GAN-based architecture.

Fig. 2 illustrates the proposed NGGAN architecture. The parameter settings for each layer are detailed in Table I, where N denotes the batch size. In the one-dimensional convolutional layer (Conv1D), the three-tuple parameter in the field "filter size" respectively indicates the length of the filter, the stride, the length of input data, and the depth of the filter. The three-tuple parameter in the "output size" denotes the batch size. The length of the feature filter is set to 25, based on an expanded two-dimensional 5×5 feature filter to observe the signals over out of range in our previous work [31], where the length of the

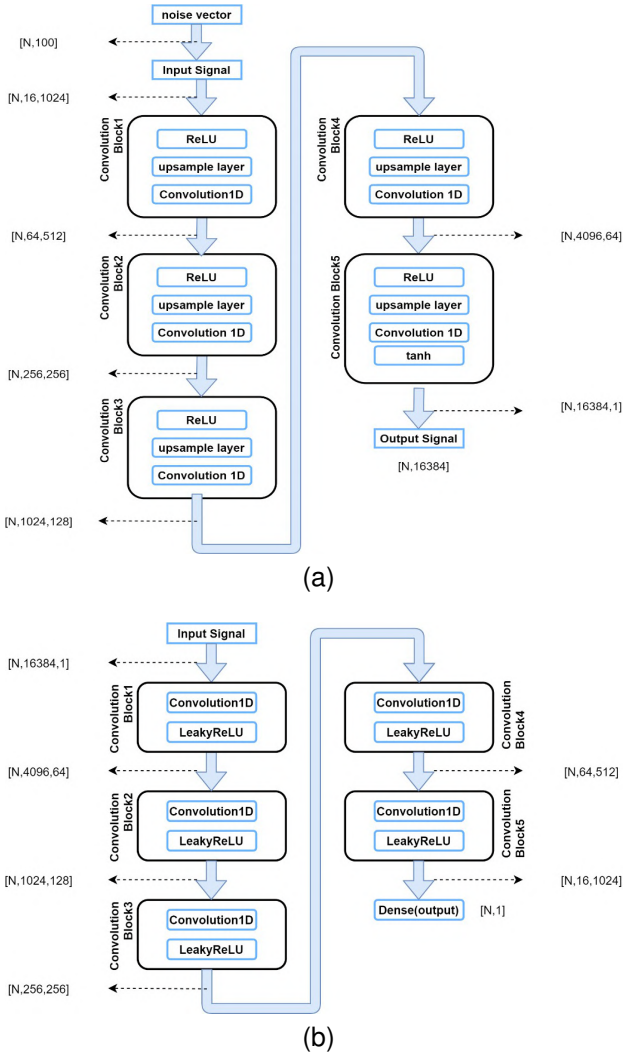

Fig. 2. The proposed NGGAN architecture: (a) generator and (b) discriminator (N is the total number of impulse noise traces).

feature filter is set to 5. It enhances the precision of learning the correlation and periodicity between noise sequences.

A. Generative Model

As shown in Fig. 2 (a), the proposed generator comprises five concatenated convolutional blocks, each of which comprises an upsampling layer with a rectified linear unit (ReLU) activation function. The details of feature filter parameters are listed in Table I (a). The input noise vector (length = 100) is sampled from a uniformly distributed random variable with a range of $[-1, 1]$. We adopted a 1D transposed convolutional layer for learning in the previous work [31].

In this study, we increase the number of layers and the length of the generated data by 4 times, resulting in the generation vector with a length of $16,384$. The block number of the generator and discriminator could depend on the application that the GAN model used. The periodic stationary impulse noise occurs with a frequency approximately half of the alternating current (AC) cycle [43], such as 8.33 ms is a cycle of impulse noise in 60 Hz AC frequency. If the sampling period is 2.5μ seconds (equivalent to $1/400$ kHz), then $16,384$ samples encompass about five cycles of the impulse noise. Thus, it grants the proposed NGGAN to capture the features or correlations extending over up to five cycles. The depth of the feature filter is reduced from 512 to 1.

In our previous work [31], the simulation results demonstrate that a transposed convolutional layer degraded upsampling learning performance because most of the interpolation values were 0. In this study, we propose a novel upsampling, combining the nearest neighbor algorithm and linear interpolation to allow the insertion of the same value in adjacent areas, thereby enlarging the signal length (by $4\times$) to preserve more information. The stride is set to 1 for the 1D convolution layer. ReLU is adopted as the activation function before each transposed convolutional layer. The hyperbolic tangent function is adopted as the activation function for the output layer to normalize values in the time-domain sequence $[-1, 1]$. A fully connected layer is used to map the noise vector to the input vector with a length of $16,384$.

TABLE I
DETAILED PARAMETERS OF EACH LAYER IN (A) GENERATOR AND (B) DISCRIMINATOR NETWORKS.

Layer name	Filter size	Activation function	Output size
Noise vector	(100, 16384)	-	(N, 100)
Input	-	-	(N, 16, 1024)
Conv1D	(25, 1, 1024, 512)	ReLU	(N, 64, 512)
Conv1D	(25, 1, 512, 256)	ReLU	(N, 256, 256)
Conv1D	(25, 1, 256, 128)	ReLU	(N, 1024, 128)
Conv1D	(25, 1, 128, 64)	ReLU	(N, 4096, 64)
Conv1D	(25, 1, 64, 1)	ReLU	(N, 16384, 1)
Output	-	tanh	(N, 16384)

(a)

Layer name	Filter size	Activation function	Output size
Input	-	-	(N, 16384, 1)
Conv1D	(25, 4,1, 64)	Leaky ReLU(0.2)	(N, 4096, 64)
Conv1D	(25, 4, 64, 128)	Leaky ReLU(0.2)	(N, 1024, 128)
Conv1D	(25, 4, 128, 256)	Leaky ReLU(0.2)	(N, 256, 256)
Conv1D	(25, 4, 256, 512)	Leaky ReLU(0.2)	(N, 64, 512)
Conv1D	(25, 4, 512, 1024)	Leaky ReLU(0.2)	(N, 16, 1024)
Dense(Output)	(16384, 1)	-	(N, 1)

(b)

B. Discriminative Model

As shown in Fig. 2 (b), the discriminator includes five convolutional layers and leaky ReLU with a parameter set 0.2. The details of the parameters of the feature filter are listed in Table I (b). By setting the stride to 4, the feature filter reduces the signal length by 4×4 layer-by-layer, such that the length of the noise vector in the first convolutional layer is reduced from $16,384$ to $4,096$. Thus, an eigenvector of length 16 is obtained through five convolution layers. The filter depth is doubled in each consecutive layer to allow the filter to learn comprehensive features from precise features. The output vector of the last layer is with size $[16, 1024]$ and the data is expanded into a vector with length $16,384$. The features are extracted by the filter and assigned weights via the fully connected layer to obtain the optimal value learned by the discriminator. The leaky ReLU activation function has a negative slope of 0.2 after each convolution.

C. Data Pre-Processing

Effective training data pre-processing and parameter initialization are essential to enhance the efficiency and accuracy of the trained model. By employing the data pre-processing techniques, we can obtain the following two advantages: (i) The first benefit is the convergence speed enhancement. It leads to the shape of the loss function being narrow and elongated, resulting in longer iteration times. The data pre-processing techniques can significantly expedite convergence speed. (ii) The second benefit is improved model accuracy. There are three data pre-processing techniques, including (1) min-max normalization, (2) Z-score standardization, and (3) PCA. By employing these three data pre-processing techniques, the subsequent stage is the selection of an appropriate loss function. The role of a loss function is to provide continuous feedback during the training process to our selected model. This feedback empowers the model to adjust its parameters and improve its performance on the given task.

IV. Performance Metrics and Training Datasets

A. Performance Metrics

Let $s_i(n)$ be the n-th samples in the i-th generated trace, each of which includes N samples $(n = 1, 2, \ldots, N)$. We evaluated the quality of the generated noise samples using the following statistical items:

1) Maximum value:

$$m_i = \max_n s_i[n]. \tag{1}$$

2) Mean value:

$$\mu_i = \frac{1}{N}\sum_{n=1}^{N} s_i[n]. \tag{2}$$

3) Energy value:

$$P_s = \frac{1}{N}\sum_{n=1}^{N} s_i^2[n]. \tag{3}$$

4) Standard deviation of the time-domain sequence:

$$\sigma_s = \sqrt{\frac{1}{N-1}\sum_{n=1}^{N}(S_i[n]-\mu_s)^2}. \tag{4}$$

5) Skewness: The asymmetry of a probability distribution is calculated by

$$S_s = \frac{\frac{1}{N}\sum_{n=1}^{N}(S_i[n]-\mu_s)^3}{(\frac{1}{N}\sum_{n=1}^{N}(S_i[n]-\mu_s)^2)^{\frac{3}{2}}}, \tag{5}$$

where a positive/negative skewness indicates that the probability density is skewed towards the right/left.

6) Kurtosis: The peak of a probability distribution is calculated by

$$K_s = \frac{\frac{1}{N}\sum_{n=1}^{N}(S_i[n]-\mu_s)^4}{(\frac{1}{N}\sum_{n=1}^{N}(S_i[n]-\mu_s)^2)^2}, \tag{6}$$

where a high peak indicates that the variance is increased by extreme outlier values.

7) Number of peaks over 0.05V: The number of peaks in a sample exceeding 0.05V is calculated by

$$NP_s = \#\{|S_i[n]| > 0.05\}, \tag{7}$$

where $\#\{\cdot\}$ denotes the counting function.

8) Skewness of auto-correlation: The auto-correlation sequence is defined as $r_k = \frac{c_k}{c_0}$, where c_k is defined as $c_k = \frac{1}{N}\sum_{n=1}^{N-k}(s_i[n]-\mu_s)(s_i[n+k]-\mu_s)$. By substituting the auto-correlation sequence r_k and its mean μ_r into (8), the sample auto-correlation skewness value SA_s is obtained by

$$SA_s = \frac{\frac{1}{N}\sum_{k=1}^{N}(r_k-\mu_r)^3}{(\frac{1}{N}\sum_{k=1}^{N}(r_k-\mu_r)^2)^{\frac{3}{2}}}. \tag{8}$$

9) Kurtosis of auto-correlation: By substituting the auto-correlation sequence r_k and its mean μ_r into (9), the auto-correlation peak value KA_s is obtained by

$$KA_s = \frac{\frac{1}{N}\sum_{k=1}^{N}(r_k-\mu_r)^4}{(\frac{1}{N}\sum_{k=1}^{N}(r_k-\mu_r)^2)^2}. \tag{9}$$

10) Cyclic spectral density (CSD) and cyclic spectral coherence (CSC): The auto-correlation of cyclo-stationary noise exhibits periodic characteristics and can be estimated from cyclic auto-correlation and cyclic power spectral density to identify the original cyclo-stationary noise [15]. Therefore, we employ CSD and CSC plots to individually examine how the intensity components of the noise change at different frequencies and their correlations. The cyclic auto-correlation function (CAF), which is expressed as follows:

$$R^{\alpha_k}[\tau] = \frac{1}{P}\sum_{n=0}^{P-1} r_k[n;\tau]e^{-j2\pi\alpha_k n}, \tag{10}$$

where $\alpha_k = k/P$, $k = 0, 1, \ldots, P-1$, denotes the k-th cyclic frequency of $r_k[n;\tau]$. The CSD function is calculated as follows

$$S[\alpha_k; f] = \sum_{\tau=-\infty}^{\infty} R^{\alpha_k}[\tau]e^{-j2\pi f\tau}, \tag{11}$$

where f represents the spectral frequency. A normalized CSD, referred to as the CSC function, is defined as follows:

$$\overline{S}[\alpha_k; f] = \frac{S(\alpha_k; f)}{\sqrt{S(0; f)S(0; f+\alpha_k)}}. \tag{12}$$

11) Principal component analysis (PCA) and Fréchet inception distance (FID): When $15,000$ data samples are generated, each data comprising eight features, where statistical features exceeding 0.05V peaks are excluded, as the primary component features for each data. The derivation of PCA is as follows. We consider a matrix $\mathbf{A}$ with dimensions 15000×8, where $\mathbf{A}_{ij}$ denotes the element in the i-th row and the j-th column. The formula for the covariance matrix $\mathbf{cov}_{kl}$ is given by

$$\mathbf{cov}_{kl} = \sum_{i=1}^{15000}(\mathbf{A}_{ik}-\mu_{A_k})(\mathbf{A}_{il}-\mu_{A_l}), \tag{13}$$

where $\mu_{A_k} = \frac{1}{15000}\sum_{i=1}^{15000}\mathbf{A}_{ik}$, and $k, l \in \{1, 8\}$. Then, we can obtain the eigenvector matrix $\mathbf{X} \in \mathbb{R}^{8\times 8}$, and $\mathbf{X}_{ij}$ denotes the i-th element in the the j-th eigenvector. Projecting

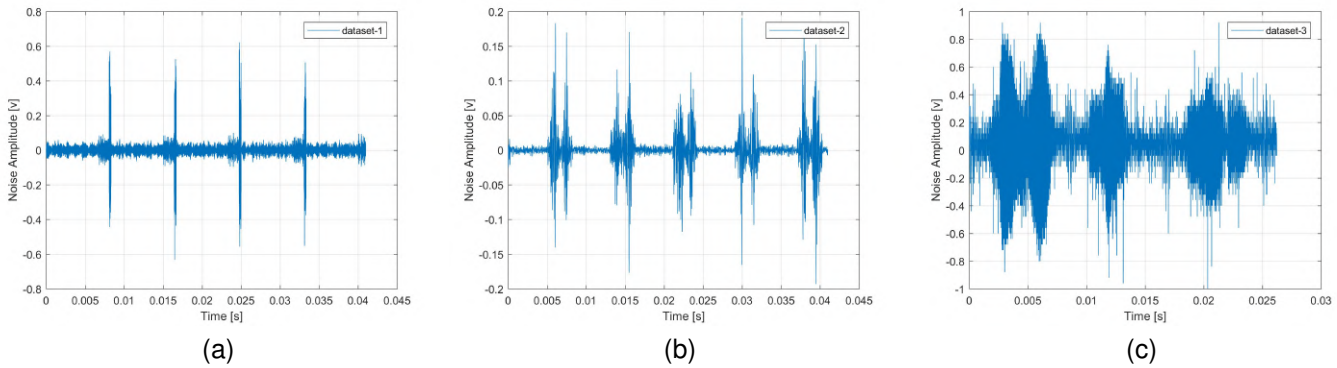

Fig. 3. Illustration of sample traces for each dataset: (a) Dataset-1, (b) Dataset-2, and (c) Dataset-3.

$\mathbf{A}$ onto the eigenvector matrix $\mathbf{X}$ yields the projection matrix $\mathbf{Y}_{qp} = \sum_{i=1}^{8} \mathbf{X}_{ip}\mathbf{A}_{qi}$, where $q = 1, 2, \ldots, 15000$, and $p = 1, 2, \ldots, 8$. Using PCA scatter, it reveals the proximity of the synthetic data distribution to real data in a 2-dimensional space and indicates whether the generated data adequately spans the area of the original data. The discrepancy between the training and generated data is treated as diversity. It facilitates the fidelity and diversity of the generated data [40].

The FID value for the noise generated by each GAN-based model is calculated by

$$\mathrm{FID}(x, g) = ||\mu_x - \mu_g||_2^2 + \mathrm{Tr}(\mathbf{\Sigma}_x + \mathbf{\Sigma}_g - 2(\mathbf{\Sigma}_x\mathbf{\Sigma}_g)^{1/2}), \quad (14)$$

where μ_x and μ_g represent the mean values of the principal component eigenvectors in the training and generated sets, respectively, while $\mathbf{\Sigma}_x$ and $\mathbf{\Sigma}_g$ refer to the covariance matrices derived from the principal component eigenvectors of the training and generated sets, respectively. A lower FID value indicates better quality and diversity of the generated data (closer to the training data distribution). Among all the performance metrics, the PCA scatter and FID values stand out as the most critical, as they effectively represent the fidelity and diversity of the generated samples.

B. Training Datasets

Based on three datasets, we compare the accuracy and diversity of several GAN-based models. Each dataset included $15,000$ records comprising $16,384$ samples (40.96ms) and is publicly accessible [35]. The first dataset is a PSCGM-generated noise trace using the parameters outlined in LV14 [18, Annex 14], which is illustrated in Fig. 3 (a). The second dataset is a FRESH-generated noise [16], which is illustrated in Fig. 3 (b). The third dataset is the real impulse noise collected using the analog coupling circuit in the front end of a commercial power-line modem development kit with a sampling rate of 625 kHz, which is illustrated in Fig. 3 (c).

Fig. 4 shows the circuits that Texas Instruments (TI) PLC Developer's Kit TIDM-TMDSPLCKIT-V3 used to measure noise for Dataset-3. To prevent the measurement circuit from being damaged, the coupling circuit is used to block the 110V/220V mains component while the power line channel is transmitting and receiving [2]. In addition, the coupling circuit

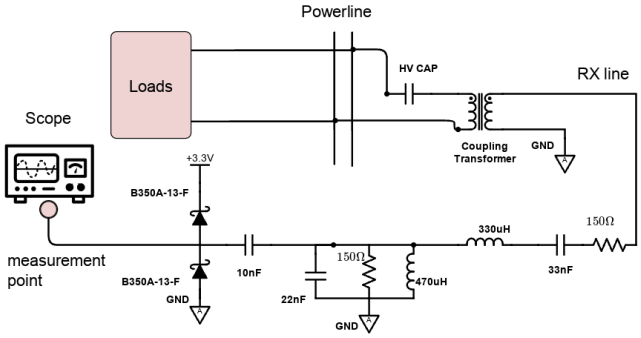

Fig. 4. The coupling circuit and analog bandpass filter in our measurement [44].

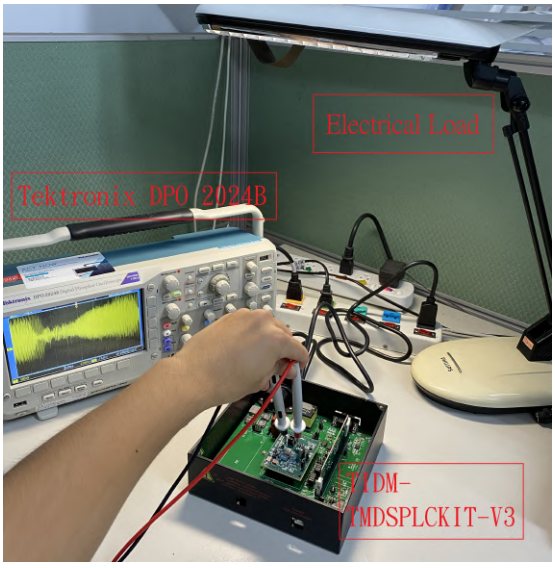

Fig. 5. Collecting the NB-PLC noise samples for Dataset-3.

is used to ensure the impedance matching of the measurement circuit and avoid the impact of voltage spikes or electrical fast transient (burst) pulses on the measurement circuit. When the PLC signal from the coupling circuit goes through a fourth-order passive bandpass filter (24 kHz to 105 kHz) by RX Line, the NB-PLC noise is measured by the Tektronix DPO 2024B

digital oscilloscope with a sampling frequency of 625 kHz.

As shown in Fig. 5, the electrical load [4] is connected to the power line to generate cyclic pulses. In total, 2.4576×10^8 sample points were collected as one piece of noise data. The total number of noise data is 15,000, and the length of each noise data is 16,384.

When collecting measurement data for Dataset-3, we considered a wide range of scenarios to ensure that Dataset-3 includes a variety of noise sample types with diverse noise characteristics. It encompassed variations in loading within the powerline network and different powerline network topologies. For example, we illustrated three scenarios involving fans, lamps, and power supplies [4] (as shown in Fig. 6). The waveforms exhibited distinct sharpness. For a more comprehensive analysis, CSD and CSC are adopted. Note that the Dataset-3 trajectories encompassed diverse scenarios, including loading across the various powerline network topologies. Therefore, Dataset-3 is more complex than the generated samples in the Dataset-1 and Dataset-2. The three datasets have been made available on IEEE DataPort [35].

V. Simulation Results

For the three datasets in Sec. IV-B, we evaluated 13 performance metrics mentioned in Sec. IV-A for the four GAN-based models, including DCGAN [30], FD-SpecGAN [37], PL-SpecGAN [31], and the proposed NGGAN in Sec. II-C. The hyperparameters setting of the four GAN-based models: learning rate 10^{-4}, epoch 200, and batch size 64 during the training process. The generated samples are examined qualitatively and quantitatively to assess the performance of GAN-based models in emulating cyclo-stationary pulse noise. To enhance the convergence rate of the proposed NGGAN model, we utilize four techniques, including the batch normalization layer, dropout, L2 regularization, and early stopping. The Python source codes for this work can be found on GitHub[2], containing comprehensive details about parameter settings.

A. Dataset-1 (PSCGM-Generated)

Fig. 7 presents the noise time series and the corresponding spectrograms for the four GAN-based models learning Dataset-1. The spectrograms reveal that the frequency components of generated noise varied periodically with time. The time series also varied periodically with time. The proposed NGGAN outperforms the other GAN-based models in terms of mean, standard deviation, and median feature statistics. NGGAN outperforms DCGAN in terms of maximum values (+9%), energy values (+34%), and standard deviation (+15%), where feature values are represented as 100% and higher values indicated greater similarity. For example, if the feature value of NGGAN-generated noise is 98% (a difference of 2%) and the feature value of DCGAN-generated noise is 88% (a difference of 12%), then the improvement afforded by NGGAN would be 10% (12% - 2%). In addition, PL-SpecGAN slightly outperforms FD-SpecGAN because it does not use the Griffin-Lim process for loss estimation.

[2]https://github.com/yrchien/NGGAN

Fig. 8 presents the CSD and CSC graph plots of noise data selected at random from Dataset-1 and noise generated by each GAN-based model. Each GAN-based model learns the correlations of cyclic frequency at frequencies of 122 Hz, 244 Hz, 366 Hz, 488 Hz, 610 Hz, and 732 Hz. However, NGGAN performs better than other GAN-based models.

Table II presents the statistical analysis of features in the noise samples generated by each GAN-based model. NGGAN outperforms other GAN-based models in seven of the nine performance metrics in Table II (a) (mean). NGGAN and DCGAN both achieve the top spot in four of the nine performance metrics in Table II (b) (standard deviation). NGGAN achieves the best performance in seven of the nine performance metrics in Table II (c). NGGAN outperforms DCGAN in terms of maximum value (+9%), energy value (+34%), and standard deviation (+15%).

Table III (a) presents the statistics of cyclic auto-correlation coefficients exceeding 0.9 of noise generated by the four GAN-based models (15,000 samples) for cyclic frequencies of 122 Hz, 244 Hz, 366 Hz, 488 Hz, 610 Hz, and 732 Hz over a frequency range of 0 to 200 kHz. The table lists the average number of auto-correlation coefficients exceeding 0.9. Since all of the cyclic auto-correlation coefficients in Dataset-1 exceed 0.9, the higher percentage of auto-correlation coefficients of generated data exceeding 0.9 indicates a higher similarity with Dataset-1. The error is calculated over a frequency range of 0 to 732 kHz. In the statistical analysis, NGGAN has the lowest accumulated error (33%).

Table III (b) presents the distribution of maximum auto-correlation coefficients. If the numbers of maximum auto-correlation coefficients of the GAN-based models are closer to Dataset-1, it indicates better learning performance in its cyclic spectral properties. Since the maximum auto-correlation coefficients of all GAN-based models are located at a cyclic frequency of 122 Hz, we focus on the maximum auto-correlation coefficient located at 244 Hz, 366 Hz, 488 Hz, 610 Hz, and 732 Hz. NGGAN outperforms other GAN-based models in four statistical quantities with errors of 5%.

Fig. 9 presents PCA scatter plots of noise generated by Dataset-1 and each GAN-based model. The X-axis and Y-axis, respectively, correspond to the first and second principal components. Thus, NGGAN is the most effective in generating noise for learning Dataset-1. The FID values in Table IV indicate that NGGAN achieved the best balance between the quality and diversity of generated noise.

B. Dataset-2 (FRESH-Generated)

Fig. 10 presents the noise time series and the corresponding spectrograms for the four GAN-based models learning Dataset-2. As the time series and spectrogram analysis in the previous sub-section (Dataset-1), the frequency components and pulse patterns in the generated noise varied cyclically with time. FD-SpecGAN model generates larger pulse values with wide waveform variations and notable statistical inconsistency. PL-SpecGAN-generated noise time series is significantly stable in terms of pulse amplitude and trajectory.

Table V presents the statistical analysis of features in the noise samples generated by each GAN-based model. NGGAN

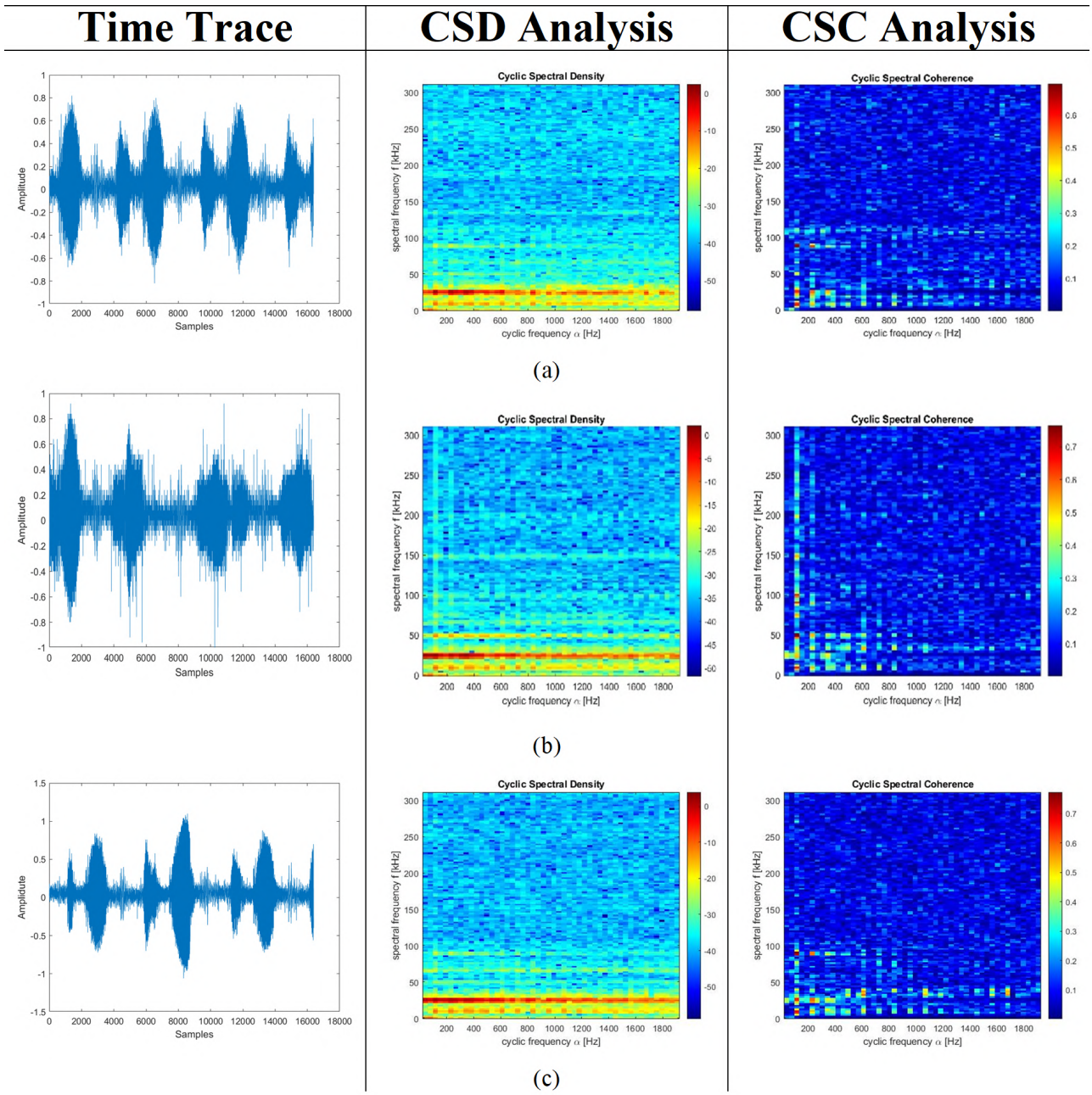

Fig. 6. Examples of various loading used when measuring noise in the NB-PLC systems: (a) Fans, (b) lamps, and (c) power suppliers.

achieves the best performance in eight of the nine performance metrics in Table V (a) (mean). NGGAN achieves the best performance in eight of the nine performance metrics in Table V (b) (standard deviation). NGGAN outperforms DCGAN in terms of maximum value (+37%), energy value (+41%), and standard deviation (+17%). Since the phase loss from the Griffin-Lim process, FD-SpecGAN-generated noise is the most unstable, resulting in the errors of maximum and energy values exceeding other GAN-based models. On the contrary, PL-SpecGAN is not affected by the phase loss of the Griffin-Lim process, which has better results than FD-SpecGAN.

In Dataset-2, the pulse noise period $T_{ac}/2$ is 1/122 second (sec), indicating a cycling frequency of 122 Hz, 244 Hz, 366 Hz, 488 Hz, 610 Hz, and 732 Hz. According to [45], the correlation coefficient of practical NB-PLC noise decreases inversely with the cycling frequency. However, the correlation coefficients of Dataset-2 noise have significant deviations from practical NB-PLC noise measurements. At 244 Hz and 366 Hz, the correlation coefficients of Dataset-2 noise are relatively low values with practical NB-PLC noise. At 488 Hz, the correlation coefficients of Dataset-2 noise are relatively high values with practical NB-PLC noise.

Fig. 11 presents the CSD and CSC graph plots of noise data selected at random from Dataset-1 and noise generated by

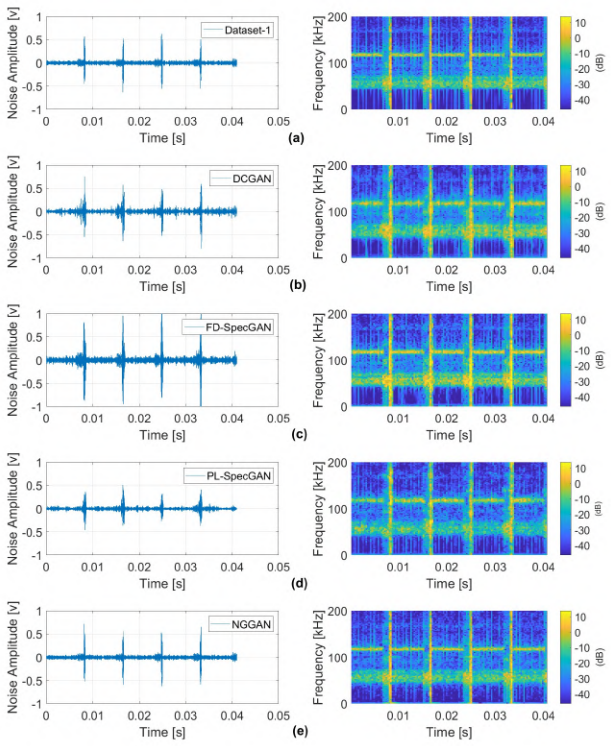

Fig. 7. Noise time series and spectrograms: (a) Dataset-1; (b) DCGAN [30]; (c) FD-SpecGAN [37]; (d) PL-SpecGAN [31]; (e) NGGAN.

each GAN-based model. The CSD and CSC graphs demonstrate that all of the GAN-based models learn well patterns associated with the cycling frequency of 122 Hz. However, the learning performances of the GAN-based models varied considerably at other cycling frequencies.

Table VI (a) presents the statistics of cyclic auto-correlation coefficients exceeding 0.5 of noise generated by the four GAN-based models (15,000 samples) for cyclic frequencies of 122 Hz, 244 Hz, 366 Hz, 488 Hz, 610 Hz, and 732 Hz. The table lists the average number of auto-correlation coefficients exceeding 0.5. By calculating the average number of correlation coefficients exceeding 0.5 over a frequency range of 0 to 200 kHz, we determine the most important features are those associated with a cycling frequency of 122 Hz. The error is calculated over a frequency range of 0 to 122 kHz. Similarly, the four GAN-based models performed well in extracting features, as indicated by the error results.

Table VI (b) presents the distribution of maximum auto-correlation coefficients. For all GAN-based models, the maximum auto-correlation coefficients are located at a cyclic frequency of 122 Hz. Therefore, we focus on the maximum auto-correlation coefficients located at 244 Hz, 366 Hz, 488 Hz, 610 Hz, and 732 Hz. It is clear that FD-SpecGAN outperforms all other GAN-based models, as indicated by the cumulative error of 7%.

Fig. 12 presents PCA scatter plots of the noise generated by Dataset-2 and each GAN-based model. The NGGAN-generated noise and PL-SpecGAN-generated noise showed the greatest similarity with Dataset-2. The FID values in Table VII show that NGGAN provided a suitable balance between the

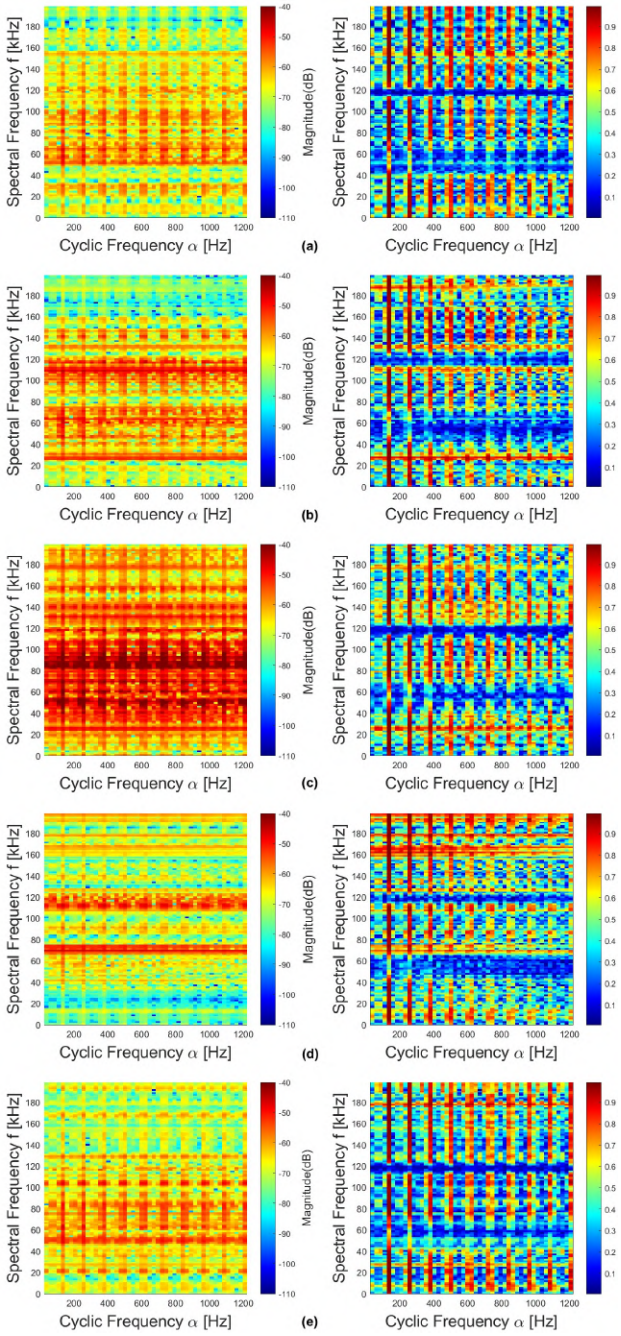

Fig. 8. CSD and CSC graphs: (a) Dataset-1; (b) DCGAN [30]; (c) FD-SpecGAN [37]; (d) PL-SpecGAN [31]; (e) NGGAN.

quality and diversity of generated noise. The FID value of PL-SpecGAN-generated noise is superior to that of FD-SpecGAN.

C. Dataset-3 (Experimentally Measured Data)

Fig. 13 presents the noise time series and the corresponding spectrograms for the four GAN-based models learning Dataset-3. The spectrograms reveal complex temporal traces with noise impulses occurring in bursts at intervals of roughly every 8.3 milliseconds over a frequency range up to 75 kHz. In addition, it shows the frequency components varied with time. However, periodic variations occur within specific frequency

TABLE II
DATASET-1 NOISE FEATURE STATISTICS: (A) MEAN, (B) STANDARD DEVIATION, AND (C) MEDIAN ANALYSIS. REFERRING TO EQS. (1) TO (9), THE FEATURES INCLUDE: (1) MAXIMUM SAMPLES [V], (2) MEAN [MV], (3) ENERGY [MJ], (4) STANDARD DEVIATION [V], (5) SKEWNESS, (6) KURTOSIS, (7) COUNT OF SAMPLES WITH PEAK $>$ 0.05 V, (8) SKEWNESS OF AUTOCORRELATION, AND (9) KURTOSIS OF AUTOCORRELATION.

Feature	Dataset-1	[30]	[37]	[31]	NGGAN
(1)	6.63E-1	7.48E-1	7.17E-1	5.23E-1	**6.46E-1**
(2)	2.14E-4	−2.74E-3	**4.81E-4**	0.928	0.887
(3)	1.79	2.51	2.38	1.46	**1.90**
(4)	4.23E-2	5.00E-2	4.75E-2	3.79E-2	**4.36E-2**
(5)	4.42E-3	−3.99E-3	**6.80E-3**	3.64E-1	−2.22E-1
(6)	60.8	41.3	45.8	34.8	**57.4**
(7)	266	630	512	399	**317**
(8)	2.59	2.24	2.37	2.35	**2.60**
(9)	10.9	9.32	9.89	9.94	**10.9**

(a)

Feature	Dataset-1	[30]	[37]	[31]	NGGAN
(1)	7.59E-2	1.21E-1	2.03E-1	1.09E-1	**6.98E-2**
(2)	1.20E-1	2.84E-1	2.78E-1	**1.21E-1**	2.95E-1
(3)	3.87E-2	**1.55E-1**	1.12	3.97E-1	1.88E-1
(4)	4.56E-4	**1.54E-3**	1.08E-2	5.06E-3	2.14E-3
(5)	4.92E-1	**4.59E-1**	4.54E-1	2.83E-1	4.02E-1
(6)	4.52	6.72	5.81	5.88	**3.79**
(7)	10.6	**37.3**	245	911	40.2
(8)	1.44E-1	1.03E-1	1.56E-1	3.58E-1	**1.46E-1**
(9)	6.94E-1	4.89E-1	7.52E-1	1.40	**7.09E-1**

(b)

Feature	Dataset-1	[30]	[37]	[31]	NGGAN
(1)	6.54E-1	7.31E-1	6.88E-1	5.0E-1	**6.40E-1**
(2)	−2.48E-4	−5.81E-3	**−1.19E-3**	9.21E-1	8.61E-1
(3)	1.79	2.50	2.14	1.41	**1.90**
(4)	4.23E-2	5.00E-2	4.63E-2	3.75E-2	**4.35E-2**
(5)	7.84E-4	−5.33E-3	**5.46E-3**	3.61E-1	−2.21E-1
(6)	60.4	40.2	45.3	34.1	**57.1**
(7)	266	629	452	387	**314**
(8)	2.59	2.24	2.37	2.36	**2.60**
(9)	10.9	9.32	9.90	9.99	**10.9**

(c)

bands. The time series reveals that burst impulses vary with time randomly. Thus, the complexity of these trace patterns made it difficult to observe structural features. The NGGAN-generated and PL-SpecGAN-generated noises show the most similarities for Dataset-3 learning.

Table VIII presents the statistical analysis of features in the noise generated by each GAN-based model. NGGAN achieved the best performance in five of the nine performance metrics in Table VIII (a) (mean), while FD-SpecGAN achieved the best performance in three of the nine performance metrics. NGGAN achieved the best performance in seven of the nine performance metrics in Table VIII (b) (standard deviation) and Table VIII (c) (median), respectively. NGGAN outperforms DCGAN in terms of the maximum value (+6%), energy value (+80%), and standard deviation (+5%). In addition, FD-SpecGAN performs better on Dataset-3 compared to Dataset-2. There are no significant differences between PL-SpecGAN and FD-SpecGAN.

Fig. 14 presents CSD and CSC plots of noise generated by each GAN-based model and noise data sampled randomly from Dataset-3. Unlike the mathematical models used for

TABLE III
STATISTICAL COMPARISONS FOR DATASET-1: (A) AUTO-CORRELATION COEFFICIENTS EXCEEDING 0.9. (B) DISTRIBUTION OF THE MAXIMUM AUTO-CORRELATION COEFFICIENT IN CYCLIC SPECTRAL AT 122 HZ.

Feature	[30]	[37]	[31]	NGGAN
122 Hz	94%	99%	96%	**100%**
244 Hz	79%	93%	84%	**96%**
366 Hz	54%	57%	55%	**94%**
488 Hz	59%	43%	49%	**93%**
610 Hz	71%	41%	58%	**92%**
732 Hz	91%	41%	74%	**92%**
Error	152%	226%	184%	**33%**

(a)

Feature	Dataset-1	[30]	[37]	[31]	NGGAN
0-50 kHz	42%	22%	40%	26%	**42%**
50-100 kHz	1%	**0%**	2%	5%	2%
100-150 kHz	6%	69%	9%	11%	**7%**
150-200 kHz	51%	9%	**48%**	57%	**48%**
Error	-	126%	9%	31%	**5%**

(b)

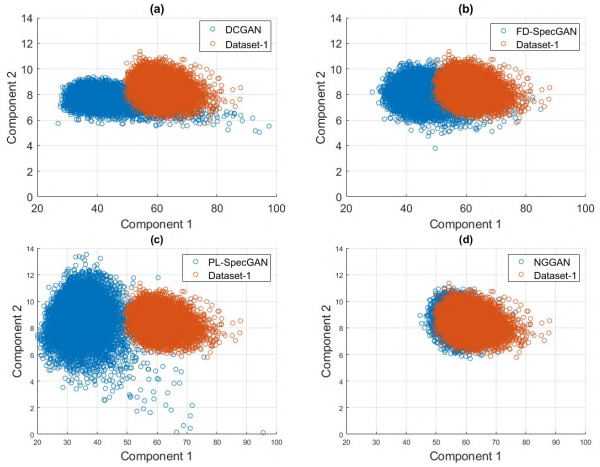

Fig. 9. PCA scatter: (a) DCGAN [30]; (b) FD-SpecGAN [37]; (c) PL-SpecGAN [31]; (d) NGGAN.

Dataset-1 and Dataset-2, the cyclo-stationary frequency of Dataset-3 is roughly 114 Hz. The four GAN-based models learned the correlation coefficients at 114 Hz, 228 Hz, 342 Hz, 456 Hz, 570 Hz, and 684 Hz. However, the learning performances at different cyclic frequencies are significantly different.

Table IX (a) presents the statistics of auto-correlation coefficients exceeding 0.3 of noise generated by the four GAN-based models generated by the four GAN-based models (15,000 samples) for cycling frequencies of 114 Hz, 228 Hz, 342 Hz, 456 Hz, 570 Hz, and 684 Hz. The error is calculated over a frequency range of 0 to 342 kHz. The table lists the average number of auto-correlation coefficients exceeding 0.3. Since

TABLE IV
PCA FEATURE FID ANALYSIS FOR DATASET-1.

DCGAN [30]	FD-SpecGAN [37]	PL-SpecGAN [31]	NGGAN
387.09	225.48	672.53	**12.16**

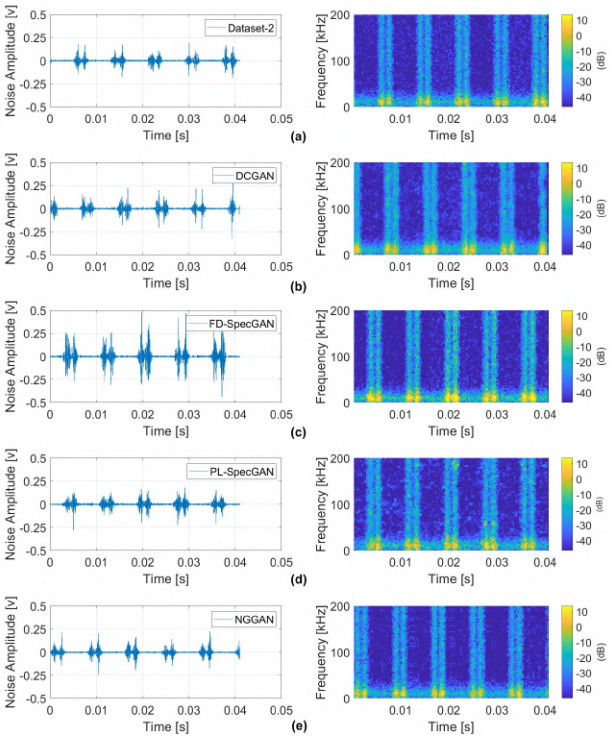

Fig. 10. Noise time series and spectrograms: (a) Dataset-2; (b) DCGAN [30]; (c) FD-SpecGAN [37]; (d) PL-SpecGAN [31]; (e) NGGAN.

all of the cyclic auto-correlation coefficients in Dataset-3 exceed 0.3, the higher percentage of auto-correlation coefficients of generated data exceeding 0.3 indicates a higher similarity with Dataset-3. In the statistical analysis, NGGAN has the lowest accumulated error (33%). Simulation results reveal that the most important features in Dataset-3 are associated with cyclo-stationary frequencies of 114 Hz, 228 Hz, and 342 Hz. FD-SpecGAN achieved the best performance cumulative error of 31%, while NGGAN achieved similar performance.

Table IX (b) presents the distribution of maximum auto-correlation coefficients. The maximum auto-correlation coefficients of four GAN-based models are located at a cyclic frequency of 114 Hz. Therefore, we focus on the maximum auto-correlation coefficients located at 228 Hz, 342 Hz, 456 Hz, 570 Hz, and 684 Hz. FD-SpecGAN outperforms the other GAN-based models for learning Dataset-3. However, NGGAN achieved a performance similar to that of FD-SpecGAN. PL-SpecGAN performs the most poorly. In Table IX (a) and (b), NGGAN outperforms DCGAN 37% and 5%, respectively.

Fig. 15 presents PCA scatter plots of noise generated by each GAN-based model and Dataset-3. The PCA scatter plots linked to FD-SpecGAN and PL-SpecGAN show heavier disparities than those associated with NGGAN. This can result in a significant deviation of the generated data from the distribution of real data, posing adverse consequences. It emphasizes the importance of balancing fidelity and diversity in GAN models. The characteristics of noise generated by NGGAN were closest to those of Dataset-3. The comparison of FID values in Table X reveals that NGGAN provided a suitable balance between the quality and diversity of generated noise.

TABLE V

DATASET-2 NOISE FEATURE STATISTICS: (A) MEAN, (B) STANDARD DEVIATION, AND (C) MEDIAN ANALYSIS. REFERRING TO EQS. (1) TO (9), THE FEATURES INCLUDE: (1) MAXIMUM SAMPLES [V], (2) MEAN [MV], (3) ENERGY [MJ], (4) STANDARD DEVIATION [V], (5) SKEWNESS, (6) KURTOSIS, (7) COUNT OF SAMPLES WITH PEAK $>$ 0.05 V, (8) SKEWNESS OF AUTOCORRELATION, AND (9) KURTOSIS OF AUTOCORRELATION.

Feature	Dataset-2	[30]	[37]	[31]	NGGAN
(1)	2.07E-1	2.86E-1	7.15E-1	1.72E-1	**2.05E-1**
(2)	−8.98E-3	3.19E-4	**-2.39E-3**	4.40E-1	−1.29E-1
(3)	5.77E-1	8.28E-1	3.13E1	4.47E-1	**5.67E-1**
(4)	2.40E-2	2.87E-2	8.74E-2	2.06E-2	**2.37E-2**
(5)	−3.35E-2	1.59E-3	2.93E-3	1.41E-1	**9.82E-3**
(6)	1.76E1	2.28E1	1.49E1	1.47E1	**1.74E1**
(7)	1.73E2	2.07E2	1.94E2	1.54E2	**1.68E2**
(8)	2.59E-1	4.32E-1	5.12E-1	3.72E-1	**2.66E-1**
(9)	1.55	1.63	2.31	1.62	**1.55**

(a)

Feature	Dataset-2	[30]	[37]	[31]	NGGAN
(1)	3.10E-2	6.63E-2	1.22	4.99E-2	**3.71E-2**
(2)	3.64E-1	1.81E-1	4.95E-1	1.74E-1	**2.95E-1**
(3)	7.99E-2	1.58E-1	1.13E2	2.03E-1	**9.37E-2**
(4)	1.66E-3	2.56E-3	1.54E-1	4.48E-3	**2.00E-3**
(5)	4.31E-1	6.59E-1	2.93E-1	2.91E-1	**4.18E-1**
(6)	2.82	7.06	4.86	3.11	**2.90**
(7)	2.17E1	**2.4E1**	1.71E2	5.66E1	42.61E1
(8)	5.15E-2	6.34E-2	6.18E-1	7.55E-2	**5.33E-2**
(9)	1.73E-2	4.20E-2	2.20	5.87E-2	**1.82E-2**

(b)

Feature	Dataset-2	[30]	[37]	[31]	NGGAN
(1)	2.05E-1	2.75E-1	**2.08E-1**	1.65E-1	22.01E-1
(2)	−8.75E-3	2.14E-5	55.57E-5	4.17E-1	−1.56E-1
(3)	5.73E-1	8.06E-1	6.06E-1	4.06E-1	**5.65E-1**
(4)	2.39E-2	2.84E-2	2.46E-2	2.01E-2	**2.38E-2**
(5)	−1.86E-2	2.32E-3	**1.27E-3**	1.35E-1	3.06E-3
(6)	1.72E1	2.12E1	1.53E1	1.43E1	**1.69E1**
(7)	1.72E2	2.05E2	1.84E2	1.51E2	**1.69E2**
(8)	2.57E-1	4.33E-1	2.95E-1	3.70E-1	**2.65E-1**
(9)	1.54	1.62	1.56	1.61	**1.55**

(c)

The proposed NGGAN consistently demonstrated superior performance compared to DCGAN, FD-SpecGAN, and PL-SpecGAN. The noise traces produced by NGGAN closely mirrored the quality and diversity of the measured dataset, establishing it as an effective model for learning and generating noise in NB-PLC communication systems. The PCA scatter diagrams confirmed that the samples generated by NGGAN can cover most of the areas obtained by each dataset. Moreover, the disparities in the generated results from the dataset showed the diversity of the NGGAN. This suggests that NGGAN achieves a favorable equilibrium between fidelity and diversity. The proposed NGGAN can be used to generate noise patterns to evaluate the robustness of the NB-PLC receivers against the complicated noise in the powerline networks [8]. Furthermore, NGGAN can be a learnable data augmentation to train artificial intelligence (AI)-based NB-PLC transceivers. The idea of the learnable data augmentation can be extended to the design of wireless consumer electronics devices that suffer from complicated noise [33], [34].

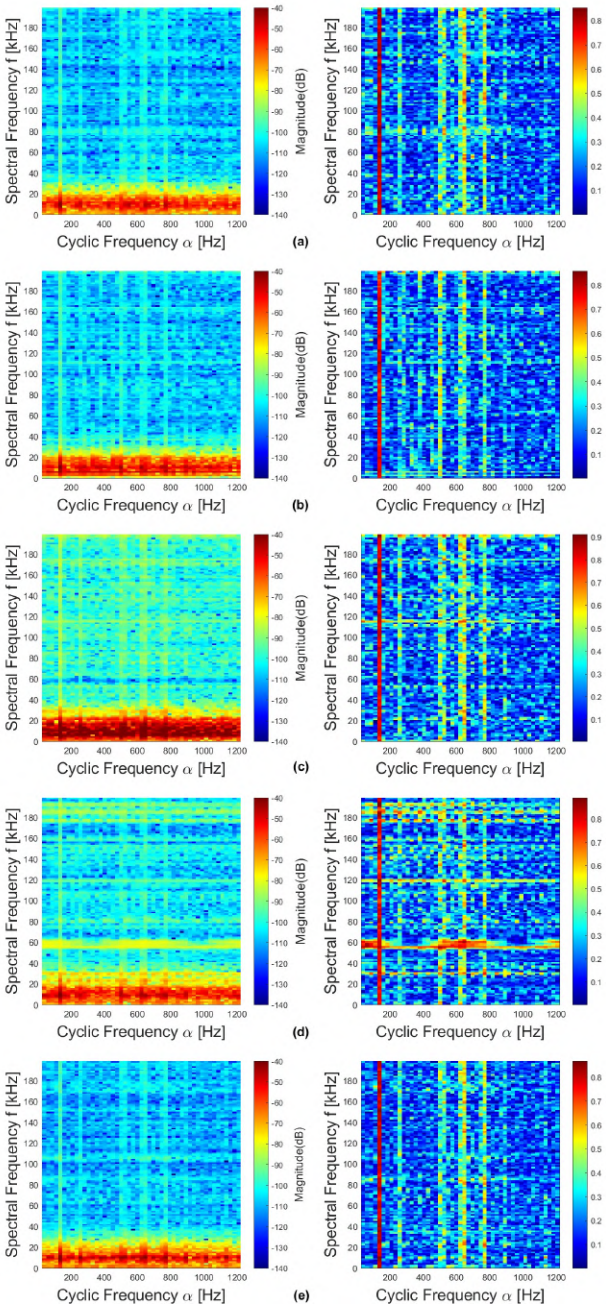

Fig. 11. CSD and CSC graphs: (a) Dataset-2; (b) DCGAN [30]; (c) FD-SpecGAN [37]; (d) PL-SpecGAN [31]; (e) NGGAN.

D. Training and Testing Time Complexity Analysis

In our simulations, Python 3.7 and its associated libraries are utilized to construct the GAN model architecture. We employed an Intel i5-7400 (CPU) and Nvidia GTX 1080Ti (GPU) as the hardware for execution. The training dataset consists of $16,384$ samples with a batch size of 32. Table XI (a) displays the time needed for training per epoch for each GAN-based model using various noise datasets. In general, DCGAN outperforms the other GAN-based models in terms of training time. However, the performance metrics of DCGAN are almost the worst overall. Notably, the proposed NGGAN demonstrates significant improvements compared to FD-SpecGAN and PL-SpecGAN in terms of training time. Table XI (b) illustrates the time required for testing per generated data for each GAN-based model using different noise datasets. In general, the trained PL-SpecGAN exhibits the shortest testing time compared to other GAN-based models. Conversely, the trained DCGAN demands the most testing time among the trained GAN-based models. The proposed NGGAN completes testing in half the time compared to the trained DCGAN.

TABLE VI
STATISTICAL COMPARISONS FOR DATASET-2: (A) AUTO-CORRELATION COEFFICIENTS EXCEEDING 0.5. (B) DISTRIBUTION OF THE MAXIMUM AUTO-CORRELATION COEFFICIENT IN CYCLIC SPECTRAL AT 122 HZ.

Feature	[30]	[37]	[31]	NGGAN
122 Hz	**100**%	96%	**100**%	**100**%
244 Hz	**112**%	138%	190%	174%
366 Hz	153%	278%	509%	**122**%
488 Hz	**100**%	98%	115%	84%
610 Hz	88%	121%	114%	**106**%
732 Hz	**111**%	266%	289%	139%
Error	**0**%	4%	**0**%	**0**%

(a)

Feature	Dataset-2	[30]	[37]	[31]	NGGAN
0-20 kHz	14%	9%	10%	2%	**12**%
20-80 kHz	30%	22%	**30**%	**30**%	20%
80-140 kHz	28%	33%	**29**%	35%	35%
140-200 kHz	29%	36%	**31**%	33%	32%
Error	-	25%	**7**%	23%	22%

(b)

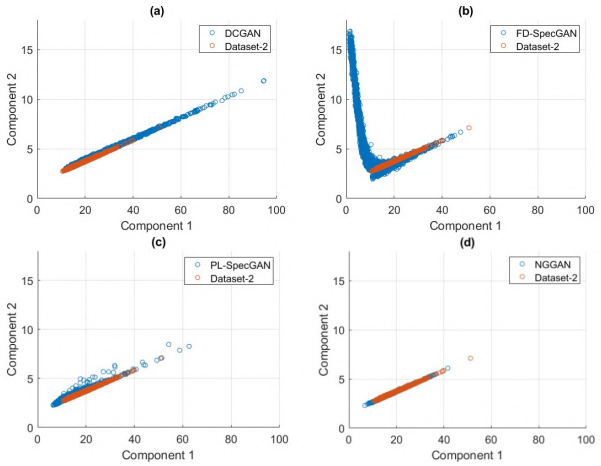

Fig. 12. PCA scatter: (a) DCGAN [30]; (b) FD-SpecGAN [37]; (c) PL-SpecGAN [31]; (d) NGGAN.

VI. CONCLUSIONS

This paper proposes an NGGAN model to learn cyclostationary noise in NB-PLC systems using two mathematically modeled noise datasets (Dataset-1 and Dataset-2) and one real

TABLE VII
PCA FEATURE FID ANALYSIS FOR DATASET-2.

DCGAN [30]	FD-SpecGAN [37]	PL-SpecGAN [31]	NGGAN
45.15	18.66	8.48	**0.07**

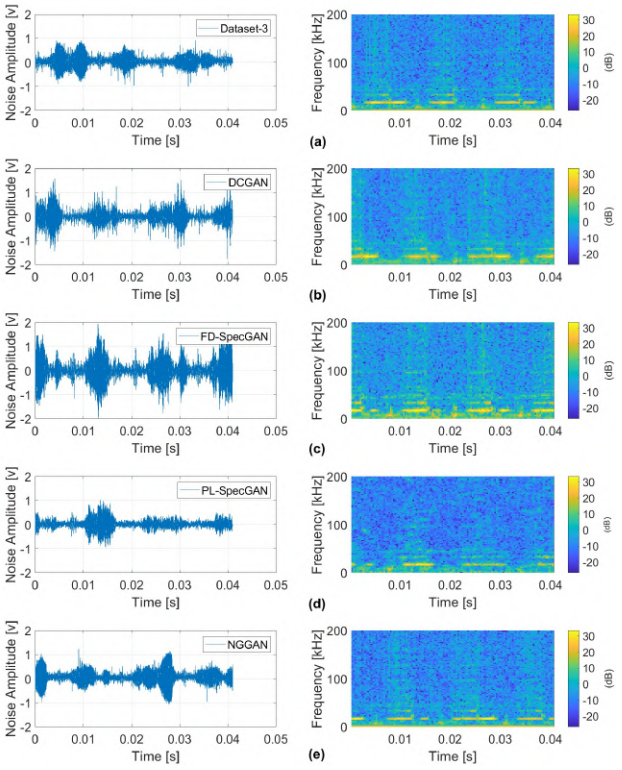

Fig. 13. Noise time series and spectrograms: (a) Dataset-3; (b) DCGAN [30]; (c) FD-SpecGAN [37]; (d) PL-SpecGAN [31]; (e) NGGAN.

measurement data (Dataset-3). We simplify the architecture of DCGAN by transforming noise data into spectrograms and extending the length of input data based on the cyclo-stationary property. Wasserstein distance is used as the loss function of the NGGAN to enhance the similarity between the generated noise and three datasets. The cyclic spectrum and diversity analysis are measured so that the generated noise ensures the inference of the data distribution of the real environment from an insufficient practical noise dataset. In our simulation, the proposed NGGAN consistently outperformed DCGAN, FD-SpecGAN, and PL-SpecGAN. Specifically, the resulting PCA scatter and FID analysis have shown that the NGGAN is able to generate higher fidelity and diversity noise samples than comparative works. Therefore, the proposed NGGAN serves as a data augmentation approach to provide the generated dataset for the design of denoising and robustness for the NB-PLC transceivers.

TABLE VIII

DATASET-3 NOISE FEATURE STATISTICS: (A) MEAN, (B) STANDARD DEVIATION, AND (C) MEDIAN ANALYSIS. REFERRING TO EQS. (1) TO (9), THE FEATURES INCLUDE: (1) MAXIMUM SAMPLES [V], (2) MEAN [MV], (3) ENERGY [MJ], (4) STANDARD DEVIATION [V], (5) SKEWNESS, (6) KURTOSIS, (7) COUNT OF SAMPLES WITH PEAK $>$ 0.05 V, (8) SKEWNESS OF AUTOCORRELATION, AND (9) KURTOSIS OF AUTOCORRELATION.

Feature	Dataset-3	[30]	[37]	[31]	NGGAN
(1)	3.33	3.96	2.01	2.16	**2.95**
(2)	2.15E2	−1.37E-2	−9.64E-3	6.84E1	**1.77E-2**
(3)	2.63E2	4.88E2	2.50E2	1.87E2	**2.52E2**
(4)	4.62E-1	6.96E-1	**4.61E-1**	4.22E-1	4.56E-1
(5)	3.21E-2	−5.39E-4	5.74E-4	**3.71E-2**	−1.84E-3
(6)	6.08E1	4.13E1	4.58E1	3.48E1	**5.74E1**
(7)	2.66E2	6.30E2	5.12E2	3.99E2	**3.17E2**
(8)	2.59	2.24	2.37	2.35	**2.60**
(9)	1.09E1	9.32	9.89	9.94	**1.09E1**

(a)

Feature	Dataset-3	[30]	[37]	[31]	NGGAN
(1)	4.46E-1	5.18E-1	7.91E-1	3.98E-1	**4.11E-1**
(2)	4.22E1	3.26	1.81	8.84	**3.03E1**
(3)	6.42E1	9.11E1	2.30E2	5.29E1	**6.57E1**
(4)	4.59E-2	6.15E-2	1.93E-1	6.05E-2	**5.75E-2**
(5)	6.72E-2	8.99E-2	5.23E-2	5.61E-2	**6.33E-2**
(6)	7.34E-1	5.00E-1	4.59E-1	8.95E-1	**6.30E-1**
(7)	2.34E2	1.28E3	1.43E2	2.02E2	**2.24E2**
(8)	1.12E-1	8.26E-2	**8.36E-2**	6.30E-2	6.74E-2
(9)	2.13E-1	2.60E-1	**2.12E-1**	1.65E-1	2.49E-1

(b)

Feature	Dataset-3	[30]	[37]	[31]	NGGAN
(1)	3.32	3.90	1.84	2.11	**2.92**
(2)	2.04E2	−5.43E-3	−7.87E-3	6.78E1	**1.67E2**
(3)	2.46E2	4.75E2	1.74E2	1.81E2	**2.30E2**
(4)	4.53E-1	6.89E-1	4.17E-1	4.20E-1	**4.49E-1**
(5)	3.24E-2	−1.53E-3	2.05E-4	**3.40E-2**	−1.53E-4
(6)	4.47	4.74	4.10	4.90	**4.23**
(7)	2.69E3	2.49E3	**2.58E3**	3.01E3	3.11E3
(8)	−1.45E-1	−1.21E-1	−1.40E-1	**-1.47E-1**	**-1.43E-1**
(9)	1.66	1.67	1.65	1.68	**1.66**

(c)

REFERENCES

[1] A. O. Aderibole, E. K. Saathoff, K. J. Kircher, A. W. Langham, L. K. Norford, and S. B. Leeb, "Characterizing low-data-rate power line communication channels," *IEEE Trans. Instrum. Meas.*, vol. 72, pp. 1–12, 2023, doi: 10.1109/TIM.2022.3225916.

[2] G. Artale, A. Cataliotti, V. Cosentino, D. D. Cara, R. Fiorelli, P. Russotto, and G. Tinè, "Medium voltage smart grid: Experimental analysis of secondary substation narrow band power line communication," *IEEE Trans. Instrum. Meas.*, vol. 62, no. 9, pp. 2391–2398, 2013, doi: 10.1109/TIM.2013.2270924.

[3] A. Cataliotti, V. Cosentino, D. Di Cara, and G. Tine, "Oil-filled MV/LV power-transformer behavior in narrow-band power-line communication systems," *IEEE Trans. Instrum. Meas.*, vol. 61, no. 10, pp. 2642–2652, 2012, doi: 10.1109/TIM.2012.2209911.

[4] M. Antoniali and A. M. Tonello, "Measurement and characterization of load impedances in home power line grids," *IEEE Trans. Instrum. Meas.*, vol. 63, no. 3, pp. 548–556, 2014.

[5] L. Angrisani, D. Petri, and M. Yeary, "Instrumentation and measurement in communication systems," *IEEE Instrum. Meas. Mag.*, vol. 18, no. 2, pp. 4–10, Apr. 2015.

[6] A. Omri, J. Hernandez Fernandez, A. Sanz, and M. R. Fliss, "PLC channel selection schemes for OFDM-based NB-PLC systems," in *IEEE Int. Symp. Power Line Commn. its Appl. (ISPLC)*, Malaga, Spain, May 2020, pp. 1–6, doi: 10.1109/ISPLC48789.2020.9115404.

[7] N. Uribe-Pérez, I. Angulo, D. de la Vega, A. Arrinda, T. Arzuaga, L. Marrón, S. Martínez, A. Sendín, and I. Urrutia, "TCP/IP capabilities over nb-plc for smart grid applications: Field validation," in *IEEE Int. Symp. Power Line Commn. its Appl. (ISPLC)*, Madrid, Spain, Apr. 2017, pp. 1–5, doi: 10.1109/ISPLC.2017.7897118.

[8] F. Rouissi, A. J. H. Vinck, H. Gassara, and A. Ghazel, "Improved impulse noise modeling for indoor narrow-band power line communication," *AEU-Int. J. Electron. Commun.*, vol. 103, pp. 74–81, May 2019, doi: 10.1016/j.aeue.2019.02.019.

[9] A. Llano, D. De La Vega, I. Angulo, and L. Marron, "Impact of channel disturbances on current narrowband power line communications and lessons to be learnt for the future technologies," *IEEE Access*, vol. 7, pp. 83 797–83 811, June 2019, doi: 10.1109/ACCESS.2019.2924806.

[10] R. R., B. Sushma, S. Gurugopinath, and R. Muralishankar, "Capacity analysis of a narrowband powerline communication channel under impulsive noise," in *2019 11th International Conference on Communication Systems Networks (COMSNETS)*, Jan. 2019, pp. 272–277.

[11] M. Zimmermann and K. Dostert, "Analysis and modeling of impul-

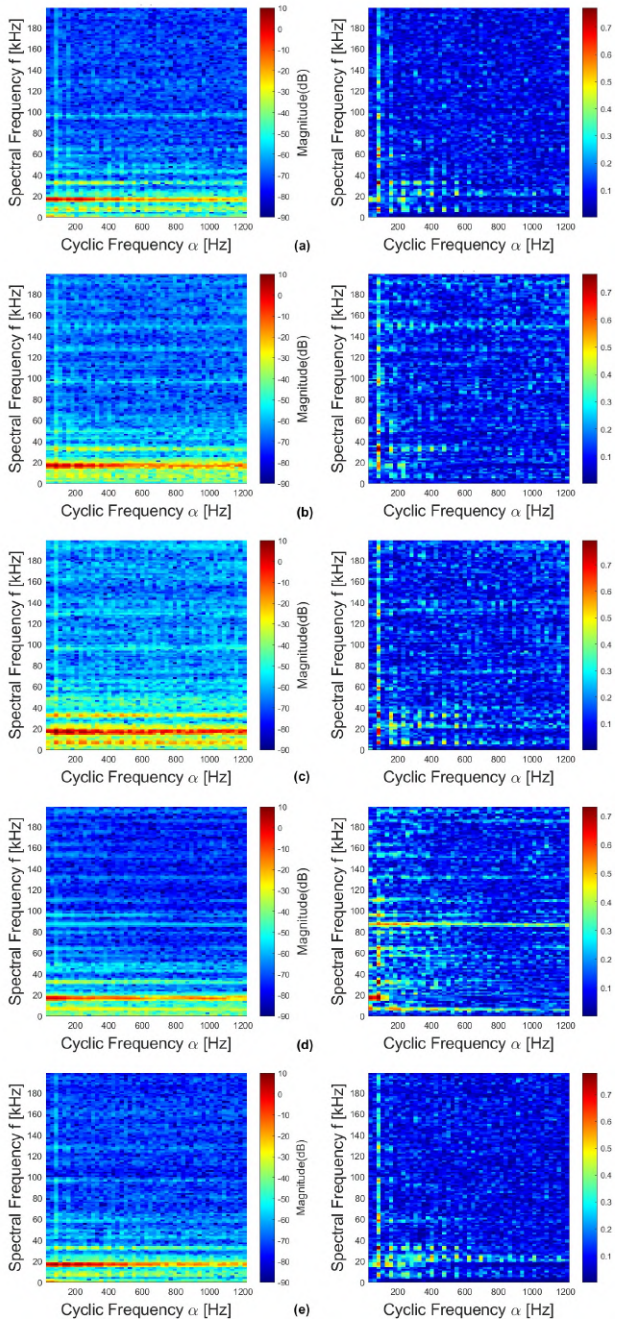

Fig. 14. CSD and CSC graphs: (a) Dataset-3; (b) DCGAN [30]; (c) FD-SpecGAN [37]; (d) PL-SpecGAN [31]; (e) NGGAN.

TABLE IX
STATISTICAL COMPARISONS FOR DATASET-3: (A) CYCLIC AUTO-CORRELATION COEFFICIENTS EXCEEDING 0.3. (B) DISTRIBUTION OF MAXIMUM VALUES OF CYCLIC AUTO-CORRELATION COEFFICIENTS IN CYCLIC SPECTRAL AT 114 HZ.

Feature	[30]	[37]	[31]	NGGAN
114 Hz	135%	**99%**	121%	105%
228 Hz	83%	89%	177%	**92%**
342 Hz	**82%**	81%	195%	80%
456 Hz	188%	97%	455%	**102%**
570 Hz	195%	97%	455%	**102%**
684 Hz	169%	**92%**	374%	193%
Error	70%	**31%**	193%	33%

(a)

Feature	Dataset-3	[30]	[37]	[31]	NGGAN
0-15 kHz	12%	0%	3%	**5%**	3%
15-35 kHz	81%	86%	**81%**	53%	84%
35-60 kHz	1%	**1%**	**1%**	3%	0%
60-200 kHz	1%	3%	**2%**	6%	**2%**
Error	-	19%	**10%**	42%	14%

(b)

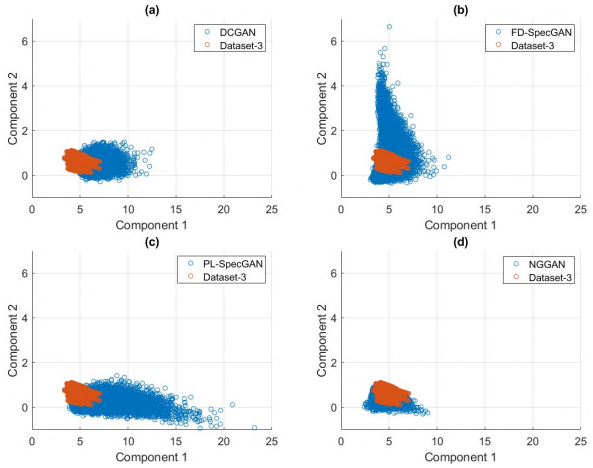

Fig. 15. PCA scatter: (a) DCGAN [30]; (b) FD-SpecGAN [37]; (c) PL-SpecGAN [31]; (d) NGGAN.

sive noise in broad-band powerline communications," *IEEE Trans. Electromagn. Compat.*, vol. 44, no. 1, pp. 249–258, Feb. 2002, doi: 10.1109/15.990732.

[12] M. Tucci, M. Raugi, L. Bai, S. Barmada, and T. Zheng, "Analysis of noise in in-home channels for narrowband power line communications," in *IEEE Int. Conf. Environ. Elect. Eng. and IEEE Ind. Commercial Power Syst. Europe (EEEIC / I & CPS Europe)*, Milan, Italy, June 2017, pp. 1–6, doi: 10.1109/EEEIC.2017.7977711.

[13] M. Katayama, T. Yamazato, and H. Okada, "A mathematical model of noise in narrowband power line communication systems," *IEEE J. Sel. Areas Commun.*, vol. 24, no. 7, pp. 1267–1276, July 2006, doi: 10.1109/JSAC.2006.874408.

[14] T. Bai, H. Zhang, J. Wang, C. Xu, M. Elkashlan, A. Nallanathan, and L. Hanzo, "Fifty years of noise modeling and mitigation in power-line communications," *IEEE Commun. Surveys Tuts.*, vol. 23, no. 1, pp. 41–69, First Quarter 2021, doi: 10.1109/COMST.2020.3033748.

[15] M. Elgenedy, M. Sayed, A. El Shafie, I. H. Kim, and N. Al-Dhahir, "Cyclostationary noise modeling based on frequency-shift filtering in NB-PLC," in *IEEE Global Commun. Conf. (GLOBECOM)*, Washington, DC, USA, 2016, pp. 1–6, doi: 10.1109/GLOCOM.2016.7841712.

[16] S. Moaveninejad, A. Kumar, M. Elgenedy, N. Al-Dhahir, A. M. Tonello, and M. Magarini, "Simpler than FRESH filter: A parametric approach for cyclostationary noise generation in NB-PLC," *IEEE Commun. Lett.*, vol. 24, no. 7, pp. 1373–1377, July 2020, doi: 10.1109/LCOMM.2020.2985130.

[17] G. Huang, D. Akopian, and C. L. P. Chen, "Measurement and characterization of channel delays for broadband power line communications," *IEEE Trans. Instrum. Meas.*, vol. 63, no. 11, pp. 2583–2590, Nov. 2014.

[18] "IEEE standard for low-frequency (less than 500 khz) narrowband power line communications for smart grid applications," *IEEE Std 1901.2-2013*, pp. 1–269, 2013, doi: 10.1109/IEEESTD.2013.6679210.

[19] I. Goodfellow, J. Pouget-Abadie, M. Mirza, B. Xu, D. Warde-Farley, S. Ozair, A. Courville, and Y. Bengio, "Generative adversarial nets," in *Advances in Neural Information Processing Systems*, vol. 27, 2014. [Online]. Available: https://proceedings.neurips.cc/paper_files/paper/2014/file/5ca3e9b122f61f8f06494c97b1afccf3-Paper.pdf

[20] S. Shirmohammadi and H. Al Osman, "Machine learning in measurement part 1: Error contribution and terminology confusion," *IEEE Instrum. Meas. Mag.*, vol. 24, no. 2, pp. 84–92, Apr. 2021.

TABLE X
PCA FEATURE FID ANALYSIS FOR DATASET-3.

DCGAN [30]	FD-SpecGAN [37]	PL-SpecGAN [31]	NGGAN
0.717	2.27	1.74	**0.24**

TABLE XI
TIME COMPLEXITY ANALYSIS: (A) TRAINING TIME PER EPOCH, AND (B) TESTING TIME PER GENERATED DATA.

Dataset	[30]	[37]	[31]	NGGAN
Dataset-1	**1 min 23 sec**	12 min 38 sec	9 min 45 sec	8 min 14 sec
Dataset-2	**2 min 29 sec**	19 min 53 sec	15 min 41 sec	7 min 6 sec
Dataset-3	**1 min 24 sec**	13 min 58 sec	15 min 58 sec	7 min 55 sec

(a)

Dataset	[30]	[37]	[31]	NGGAN
Dataset-1	0.02 sec	0.005 sec	**0.003 sec**	0.01 sec
Dataset-2	0.02 sec	0.005 sec	**0.003 sec**	0.01 sec
Dataset-3	0.02 sec	0.005 sec	**0.003 sec**	0.01 sec

(b)

[21] M. Khanafer and S. Shirmohammadi, "Applied AI in instrumentation and measurement: The deep learning revolution," *IEEE Instrum. Meas. Mag.*, vol. 23, no. 6, pp. 10–17, Sept. 2020.

[22] H. Loschi, D. Nascimento, R. Smolenski, W. E. Sayed, and P. Lezynski, "Shaping of converter interference for error rate reduction in PLC-based smart metering systems," *Measurement*, vol. 203, p. 111946, Nov. 2022.

[23] M. Elgenedy, M. Sayed, N. Al-Dhahir, and R. C. Chabaan, "Cyclostationary noise mitigation for simo powerline communications," *IEEE Access*, vol. 6, pp. 5460–5484, Jan. 2018.

[24] S. Raponi, J. H. Fernandez, A. Omri, and G. Oligeri, "Long-term noise characterization of narrowband power line communications," *IEEE Trans. Power Del.*, vol. 37, no. 1, pp. 365–373, Feb. 2022.

[25] P. S. Sausen, A. Sausen, M. De Campos, L. F. Sauthier, A. C. Oliveira, and R. R. Emmel Júnior, "Power line communication applied in a typical brazilian urban power network," *IEEE Access*, vol. 9, pp. 72 844–72 856, May 2021.

[26] R. Alaya and R. Attia, "Narrowband powerline communication measurement and analysis in the low voltage distribution network," in *2019 International Conference on Software, Telecommunications and Computer Networks (SoftCOM)*, Sept. 2019, pp. 1–6.

[27] Y.-R. Chien, J.-L. Lin, and H.-W. Tsao, "Cyclostationary impulsive noise mitigation in the presence of cyclic frequency offset for narrowband powerline communication systems," *Electronics*, vol. 9, no. 6, 2020.

[28] H. Al Osman and S. Shirmohammadi, "Machine learning in measurement part 2: Uncertainty quantification," *IEEE Instrum. Meas. Mag.*, vol. 24, no. 3, pp. 23–27, May 2021.

[29] C. Pandey, V. Tiwari, A. L. Imoize, C.-T. Li, C.-C. Lee, and D. S. Roy, "5GT-GAN: Enhancing data augmentation for 5G-enabled mobile edge computing in smart cities," *IEEE Access*, vol. 11, pp. 120 983–120 996, Oct. 2023, doi: 10.1109/ACCESS.2023.3328170.

[30] N. A. Letizia, A. M. Tonello, and D. Righini, "Learning to synthesize noise: The multiple conductor power line case," in *IEEE Int. Symp. Power Line Commn. its Appl. (ISPLC)*, Malaga, Spain, June 2020, pp. 1–6, doi: 10.1109/ISPLC48789.2020.9115394.

[31] Y.-R. Chien, Y.-J. Peng, and H.-W. Tsao, "GAN-based cyclostationary noise generator for narrowband powerline communication systems," in *Intell. Signal Process. Commun. Syst. (ISPACS)*, Hualien City, Taiwan, Nov. 2021, pp. 1–2, doi: 10.1109/ISPACS51563.2021.9651120.

[32] A. M. Tonello, N. A. Letizia, D. Righini, and F. Marcuzzi, "Machine learning tips and tricks for power line communications," *IEEE Access*, vol. 7, pp. 82 434–82 452, June 2019, doi: 10.1109/ACCESS.2019.2923321.

[33] J. Lemley and P. Corcoran, "Deep learning for consumer devices and services 4—a review of learnable data augmentation strategies for improved training of deep neural networks," *IEEE Consum. Electron. Mag.*, vol. 9, no. 3, pp. 55–63, 2020, doi: 10.1109/MCE.2019.2959075.

[34] S. Sharma, V. Bhatia, and A. K. Mishra, "Wireless consumer electronic devices: The effects of impulsive radio-frequency interference," *IEEE Consum. Electron. Mag.*, vol. 8, no. 4, pp. 56–61, July 2019, doi: 10.1109/MCE.2019.2905538.

[35] Y.-R. Chien, P.-H. Chou, Y.-J. Peng, C.-Y. Huang, H.-W. Tsao, and Y. Tsao, "Cyclostationary impulse noise dataset," 2023. [Online]. Available: https://dx.doi.org/10.21227/a1ns-hq82

[36] M. H. Hayes, *Statistical digital signal processing and modeling*. John Wiley Sons, 1996.

[37] A. Radford, L. Metz, and S. Chintala, "Unsupervised representation learning with deep convolutional generative adversarial networks," in *Int. Conf. Learn. Representations*, 2016. [Online]. Available: http://arxiv.org/abs/1511.06434

[38] I. Gulrajani, F. Ahmed, M. Arjovsky, V. Dumoulin, and A. Courville, "Improved training of Wasserstein GANs," in *Proc. Int. Conf. Neural Info. Process. Syst.*, 2017, p. 5769–5779. [Online]. Available: https://dl.acm.org/doi/pdf/10.5555/3295222.3295327

[39] C. Donahue, J. McAuley, and M. Puckette, "Adversarial audio synthesis," 2018. [Online]. Available: https://arxiv.org/abs/1802.04208

[40] J. Yoon, D. Jarrett, and M. van der Schaar, "Time-series generative adversarial networks," in *Advances in Neural Information Processing Systems*, vol. 32, Vancouver, Canada, Dec. 2019, pp. 1–11. [Online]. Available: https://proceedings.neurips.cc/paper_files/paper/2019/file/c9efe5f26cd17ba6216bbe2a7d26d490-Paper.pdf

[41] J. Stanczuk, C. Etmann, L. M. Kreusser, and C.-B. Schönlieb, "Wasserstein GANs work because they fail (to approximate the wasserstein distance)," *ArXiv*, vol. abs/2103.01678, 2021. [Online]. Available: https://api.semanticscholar.org/CorpusID:232092585

[42] D. Griffin and J. Lim, "Signal estimation from modified short-time Fourier transform," *IEEE Trans. Acoust., Speech, Signal Process.*, vol. 32, no. 2, pp. 236–243, Apr. 1984, doi: 10.1109/TASSP.1984.1164317.

[43] D. Cooper and T. Jeans, "Narrowband, low data rate communications on the low-voltage mains in the CENELEC frequencies. I. noise and attenuation," *IEEE Trans. Power Delivery*, vol. 17, no. 3, pp. 718–723, July 2002, doi: 10.1109/TPWRD.2002.1022794.

[44] T. Instruments, "TIDM-TMDSPLCKIT-v3 reference design," 2014, [Online] available: https://www.electronicsdatasheets.com/manufacturers/texas-instruments/reference-designs/TIDM-TMDSPLCKIT-V3.

[45] K. F. Nieman, J. Lin, M. Nassar, K. Waheed, and B. L. Evans, "Cyclic spectral analysis of power line noise in the 3–200 kHz band," in *IEEE Int. Symp. Power Line Commn. its Appl. (ISPLC)*, Johannesburg, South Africa, Mar. 2013, pp. 315–320, doi: 10.1109/ISPLC.2013.6525870.

Ying-Ren Chien (Senior Member, IEEE) received the B.S. degree in electronic engineering from the National Yunlin University of Science and Technology, Douliu, Taiwan, in 1999, and the M.S. degree in electrical engineering and the Ph.D. degree in communication engineering from National Taiwan University, Taipei, Taiwan, in 2001 and 2009, respectively. In 2012, Dr. Chien joined the Department of Electrical Engineering, National Ilan University, Yilan City, Taiwan. Since 2018, he has been promoted to Full Professor and served as the Chair. Since 2022, he has been the vice chair of IEEE CESoc Virtual Reality, Augmented Reality, and Metaverse (VAM). Dr. Chien is currently an Associate Editor for the IEEE TRANSACTIONS ON CONSUMER ELECTRONICS. He received Best Paper Awards, including ICCCAS 2007, ROCKLING 2017, and IEEE ISPACS 2021. Dr. Chien was presented with the IEEE CESoc/CTSoc Service Awards (2019), NSC/MOST Special Outstanding Talent Award (2021, 2023), Excellent Research-teacher Award (2018 and 2022), and Excellent Teaching Award (2021). His research interests are consumer electronics, multimedia denoising algorithms, adaptive signal processing theory, active noise control, machine learning, Internet of Things, and interference cancelation.

Po-Heng Chou (Member, IEEE) was born in Tainan, Taiwan. He received the B.S. degree in electronic engineering from National Formosa University (NFU), Huwei, Yunlin, Taiwan, in 2009, the M.S. degree in communications engineering from National Sun Yatsen University (NSYSU), Kaohsiung, Taiwan, in 2011, and the Ph.D. degree from the Graduate Institute of Communication Engineering (GICE), National Taiwan University (NTU), Taipei, Taiwan, in 2020. He is currently a Postdoctoral Fellow at the Research Center for Information Technology Innovation (CITI), Academia Sinica, Taipei, Taiwan. His research interests include deep learning-based signal processing, wireless communications, and wireless networks. Dr. Chou received the Outstanding University Youth Award and the Phi Tau Phi Honorary Membership from NTU in 2019 to honor his impressive academic achievement. He received the Ph.D. Scholarships from the Chung Hwa Rotary Educational Foundation from 2019 to 2020. Additionally, he has been elected as the Distinguished Postdoctoral Scholar of CITI by Academia Sinica from Jan. 2022 to Dec. 2023. He is invited to visit Virginia Tech (VT) Research Center, Arlington, VA, USA, as a Visiting Fellow, from Aug. 2023 to Feb. 2024. He received the Partnership Program for the Connection to the Top Labs in the World (Dragon Gate Program) from the National Science and Technology Council (NSTC) of Taiwan to perform advanced research at VT Research Center from 2024 to 2026.

You-Jie Peng was born in Beipu, Hsinchu City, Taiwan, in 1996. He received the B.E. degree from National Taipei University (NTPU), Taipei, Taiwan, in 2020 and the M.S. degree from the Graduate Institute of Communication Engineering (GICE), National Taiwan University (NTU), Taipei, Taiwan, in 2022. His current research interests include deep learning, statistical signal processing, and powerline communications. He won the Best Paper Award of the International Symposium on Intelligent Signal Processing and Communication Systems (ISPACS) in 2021.

Chun-Yuan Huang was born in Changhua, Taiwan, in 2000. He received the B.S. degree in computer and communications engineering from the National Kaohsiung University of Science and Technology (NKUST), Kaohsiung, in 2022, and the M.S. degree in communications engineering from National Sun Yat-sen University (NSYSU), Kaohsiung in 2024. His research interests include deep learning for wireless communications and communication theory.

Hen-Wai Tsao was born in Taipei, Taiwan, in 1953. He received the B.S., M.S., and Ph.D. degrees from National Taiwan University (NTU), Taipei, Taiwan, in 1975, 1978, and 1990, respectively, all in electrical engineering. Since 1978, he has been with the Department of Electrical Engineering, National Taiwan University, where he is currently a Professor Emeritus. His main research interests include broadband communication systems, communication electronics, instrumentation systems, and related electronic circuits.

Yu Tsao (Senior Member, IEEE) received his B.S. and M.S. degrees in Electrical Engineering from National Taiwan University, Taipei, Taiwan, in 1999 and 2001, respectively, and his Ph.D. degree in Electrical and Computer Engineering from the Georgia Institute of Technology, Atlanta, GA, USA, in 2008. From 2009 to 2011, he was a researcher at the National Institute of Information and Communications Technology, Kyoto, Japan, where he worked on research and product development in automatic speech recognition for multilingual speech-to-speech translation. He is currently a Research Fellow (Professor) and the Deputy Director of the Research Center for Information Technology Innovation at Academia Sinica, Taipei, Taiwan. He also serves as a Jointly Appointed Professor in the Department of Electrical Engineering at Chung Yuan Christian University, Taoyuan, Taiwan. His research interests include assistive oral communication technologies, audio coding, and bio-signal processing. Dr. Tsao is currently an Associate Editor for the IEEE/ACM TRANSACTIONS ON AUDIO, SPEECH, AND LANGUAGE PROCESSING and IEEE SIGNAL PROCESSING LETTERS. He was the recipient of the Academia Sinica Career Development Award in 2017, National Innovation Awards from 2018 to 2021, the Future Tech Breakthrough Award in 2019, the Outstanding Elite Award from the Chung Hwa Rotary Educational Foundation in 2019–2020, the NSTC FutureTech Award in 2022, and the NSTC Outstanding Research Award in 2023. He is the corresponding author of a paper that received the 2021 IEEE Signal Processing Society (SPS) Young Author Best Paper Award.